

Article

An Improved MbICP Algorithm for Mobile Robot Pose Estimation

Lin Li ^{1,2} , Jun Liu ¹, Xinkai Zuo ¹ and Haihong Zhu ^{1,*}

¹ School of Resources and Environmental Science, Wuhan University, 129 Luoyu Road, Wuhan 430079, China; lilin@whu.edu.cn (L.L.); 2011301130092@whu.edu.cn (J.L.); zuoxinkai2012@whu.edu.cn (X.Z.)

² Collaborative Innovation Center of Geo Spatial Technology, Wuhan University, 129 Luoyu Road, Wuhan 430079, China

* Correspondence: hhzhu@whu.edu.cn; Tel.: +86-27-6877-8879

Received: 20 December 2017; Accepted: 6 February 2018; Published: 12 February 2018

Featured Application: The metric-based iterative closest point algorithm is frequently used for mobile robot pose estimation by scan matching. The improved version can be used for matching scans that partially overlap.

Abstract: This paper presents an improved version of the metric-based iterative closest point algorithm to estimate robot poses by matching 2D laser scans with different overlapping percentages. Because of the greatly varied density distribution of realistic point clouds, a resampling method is used to accelerate the iteration process and protect the calculation of the rejection threshold from being distorted by reducing dense but unhelpful points. A new procedure that combines point-to-point and point-to-line metrics is used to determine the correct correspondence between partially overlapping scans, which maintains both efficiency and accuracy. In addition, a rejection threshold that is based on the MAD-from-median method is utilized to discard correspondences with large distances, which are likely to be incorrect. Experiments show that the improved algorithm is more accurate and robust than the standard algorithm with respect to the existence of non-overlapping areas, and testing demonstrates that it is valid in practice.

Keywords: 2D laser scans; robot pose; resampling; partially overlapping

1. Introduction

Simultaneous localization and mapping (SLAM) is one of the most important issues in mobile robotics research [1–5]. SLAM is a process by which a mobile robot can build a map of its environment and simultaneously use this map to locate itself [6]. Therefore, an accurate motion estimation of the robot will greatly facilitate the realization of this process and has attracted considerable attention from researchers in recent decades [1,2,7–9].

Scan-matching techniques are widely used to estimate mobile robot motion by matching successive range measurements from a laser range finder (LRF) [1,2,4,9–17]. The iterative closest point (ICP) algorithm is one of the most popular scan-matching techniques because of its efficiency and simplicity [18–22]. This algorithm iteratively establishes correspondences based on the criterion of the closest point and calculates a rigid transformation that minimizes the distance error until convergence. However, ICP tends to fall into local optima when large sensor rotation is introduced, which frequently arises when a robot rotates around itself or unexpected slippage occurs [1]. Additionally, ICP utilizes a point-to-point metric to determine correspondences, which is less accurate because of the discreteness of laser scans. In addition, ICP relies on a questionable assumption that successive scans perfectly overlap [19,20], which can hardly stand because of changes in the environment and occlusions from

vehicle motion [3,20,23]. False correspondences will arise in non-overlapping areas and thus cause the algorithm to converge upon an incorrect solution [20].

To solve the problem of scan matching with large rotation, Minguez proposed a metric-based ICP algorithm (MbICP) [10] that establishes correspondences and calculates transformations based on its defined metric-based distance, which simultaneously considers both translation and rotation. This algorithm is claimed [1,2,10] to be robust and accurate when the rotation change is large but still limited to matching scans that perfectly overlap.

Considerable research has been conducted to improve ICP and its variants in matching partially overlapping scans by enhancing the performance of correspondence establishment and rejecting incorrect correspondences [19,20,22–26]. In terms of establishing correspondence, Chen proposed a point-to-plane approach, which determines the correspondence by finding the projection of the source point onto the tangent plane at a destination surface point that is the intersection of the normal vector of the source point [27], but this approach is only available for scan matching with three-dimension (3D) laser scans. Zhang proposed a biunique correspondence ICP (BC-ICP) [20], which guarantees unique correspondence by searching for multiple closest points instead of one point. However, this strategy assumes that the corresponding point search begins from an overlapping area, which cannot be guaranteed in practice. In terms of rejecting incorrect correspondences, Druon proposed a rejection strategy that was based on a statistical analysis of the correspondence distance, which adopted $\mu + \sigma$ as the rejection threshold [28–30]. Nevertheless, this strategy assumes that the distribution of distances is Gaussian, which is not a reasonable assumption in a dynamic environment [22]. Chetverikov proposed a trimmed ICP algorithm (TrICP) [26], which uses golden-section searching to estimate an overlapping ratio and uses a trimmed least-squares approach to discard incorrect correspondence pairs. Despite the claimed robustness of this algorithm, TrICP is time consuming because it repeatedly searches for the best overlapping ratio [22,24]. This algorithm may also be misled by a large change in the overlap because of occlusions from a moving platform. Pomerleau proposed an adaptive rejection technique called the relative motion threshold (RMT) [22], which calculates the rejection threshold with a simulated annealing ratio. This technique is flawed in that the rejection threshold heavily relies on the translation vector, so a large sensor rotation may produce an incorrect rejection [20].

This paper proposes an improved MbICP algorithm for mobile robot pose estimation by using partially overlapping laser scans from a 2D laser scanner, which is commonly used because of its low cost and effectiveness in terms of data processing. Before matching, a resampling step is executed in the object scan to make the density distribution of point clouds relatively even. In terms of scan matching, finding the nearest point is still based on a metric distance, but the procedure of determining the correspondence is improved by combining the point-to-point and point-to-line metrics. Then, a distance threshold that is based on the MAD-from-median method is calculated to reject correspondences with distances above the threshold. Experiments are designed to compare the performance of the improved algorithm and standard algorithm in terms of robustness, accuracy and convergence. Furthermore, a series of real-world experiments are conducted to test its validity in realistic situations.

The paper is organized as follows. In Section 2, the principle of the ICP algorithm and the metric-based distance as defined by MbICP are outlined, followed by a detailed explanation of the resampling method and improved algorithm. The experimental results are presented in Section 3 and discussed in Section 4. The last section describes several conclusions.

2. Scan-Matching Algorithm

2.1. ICP Algorithm

Robot motion between time steps can be represented by a transformation vector T , which consists of a translation component $\Delta t = (\Delta x, \Delta y)$ and a rotational component $\Delta \theta$. Given two successive scans

from a laser scanner at the beginning and end of motion, the first scan is marked as the reference scan S_{ref} and the second scan is treated as the object scan S_{obj} (as shown in Figure 1b).

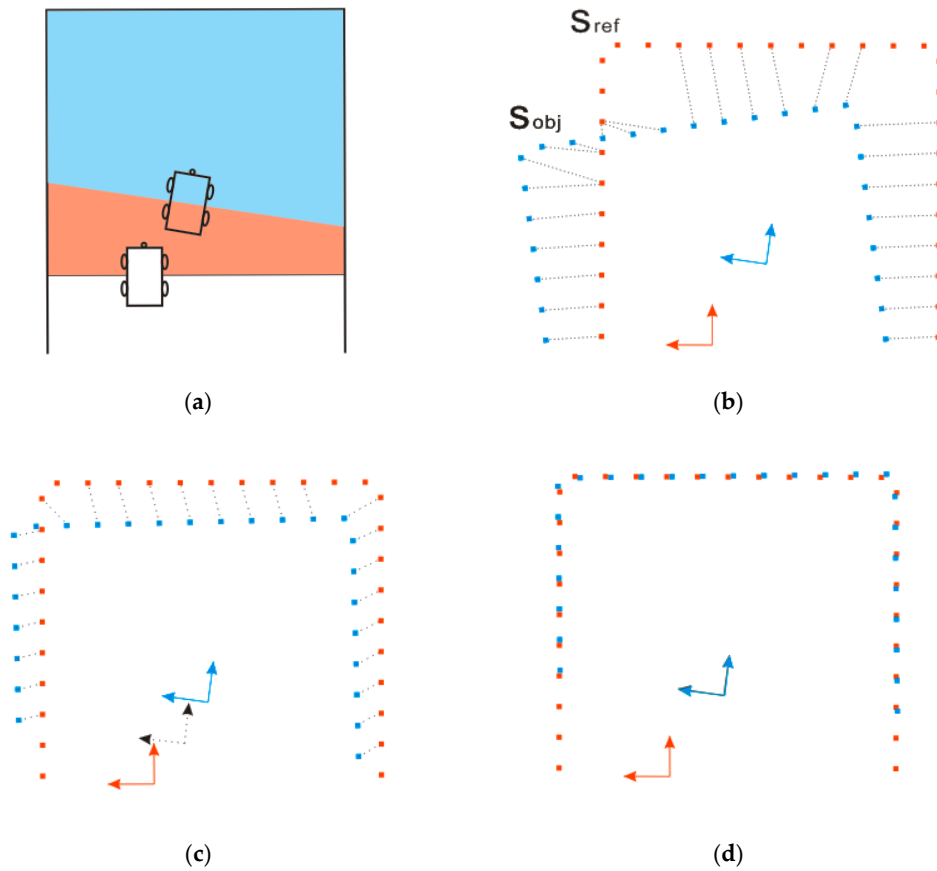


Figure 1. (a) Two laser scans that were taken at times t_1 and t_2 ; (b) object scan S_{obj} (blue) that was taken at t_2 is represented in the coordinate system of the reference scan S_{ref} (red), and the dotted lines are the correspondences based on the criterion of the closest point; (c) S_{obj} (blue) is brought closer to S_{ref} (red) as the iterations progress; (d) S_{obj} (blue) closely fits to S_{ref} (red) at the end of the iteration process.

The transformation T can be estimated by minimizing the distance of the corresponding points between S_{ref} and S_{obj} with the ICP algorithm, which is based on a three-step iterative process:

1. Establish correspondence. For each point in S_{obj} , search for the closest point in S_{ref} to establish correspondence. A K-D tree is recommended to accelerate the searching process.
2. Calculate the transformation. The rigid transformation T consisting of rotation matrix R and translation vector t is calculated by minimizing the mean square error of the correspondence pairs between S_{obj} and S_{ref} (Equation (1)). SVD-based least-squares minimization is commonly used because of its robustness and simplicity [31].

$$T = (R, t) = \operatorname{argmin} \left\{ \sum_{i=1}^N |m_j - R p_i - t|^2 \right\} \quad (1)$$

where N is the number of points in S_{obj} , $p_i \in S_{obj}$ and $m_j \in S_{ref}$. m_j is the closest point of p_i , which is defined as the correspondence.

3. Transform S_{obj} . Apply a rigid transformation to S_{obj} and update the related parameters.

These three steps are repeated until convergence or the iteration number exceeds the maximum number of iterations.

2.2. Metric-based Distance

Assume that two successive laser scans with large rotation are given (Figure 2): the reference scan S_{ref} with n_p points, $P = \{p_i, i = 1, \dots, n_p\}$, and the object scan S_{obj} with n_m points, $M = \{m_j, j = 1, \dots, n_m\}$. When establishing the correspondence, the standard ICP algorithm searches for the closest point in M for each point in P , which is under the framework of Euclidean space. Points in P that are far from the center are also far from their actual correspondence points because of the angular difference, which easily creates false correspondence and ICP failure. Thus, finding the closest point in Euclidean space is not reliable for establishing correspondence when large rotation exists.

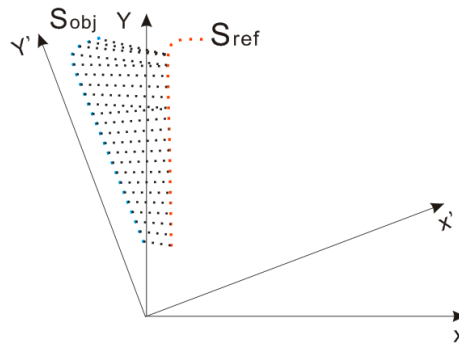


Figure 2. Two scans that were captured at the beginning and end of robot motion. The blue scan is the object scan (S_{obj}) and the red scan is the reference scan (S_{ref}). The dotted lines are the correspondence based on the criterion of the closest point.

To overcome the defect of Euclidean distance in merely considering the translation component, MbICP defines a new distance measure called the metric-based distance, which simultaneously considers both translation and rotation. Given two points in R^2 , the reference point $p_i = (p_{ix}, p_{iy})$ and the object point $m_j = (m_{jx}, m_{jy})$. A set of rigid-body transformations $q = (x, y, \theta)$ can be acquired that satisfies $q(m_j) = p_i$ (Equation (2)).

$$q(m_j) = \begin{pmatrix} x + \cos\theta \times p_{1x} - \sin\theta \times p_{1y} \\ y + \sin\theta \times p_{1x} + \cos\theta \times p_{1y} \end{pmatrix} \quad (2)$$

The metric distance $d(p_i, m_j)$ between m_j and p_i is defined as the minimum norm among the transformations (Equation (3)).

$$d(p_i, m_j) = \min\{\text{norm}(q), q(m_j) = p_i\} \quad (3)$$

where

$$\text{norm}(q) = \sqrt{x^2 + y^2 + \theta^2 L^2} \quad (4)$$

L is a balance parameter that is homogeneous to a length, which is used to balance the translational and rotational components.

A set of iso-distance curves relative to P_i and M_j is depicted by using the metric-based distance and Euclidean distance to visually represent the geometric features of metric-based distance (Figure 3a). The iso-distance curves that use the metric-based distance are claimed to be ellipses in the literature [10], while those that use the Euclidean distance are inscribed circles, which provides the metric-based distance a larger search zone than that of the Euclidean distance for the same search radius. The farther the object point is from the center, the longer the long axis of the ellipse becomes and, therefore, the more likely the object point will find its correspondence point in the rotational direction. This feature of the metric-based distance improves the probability of finding the correct correspondence for points that are far from the sensor, as shown in Figure 3b.

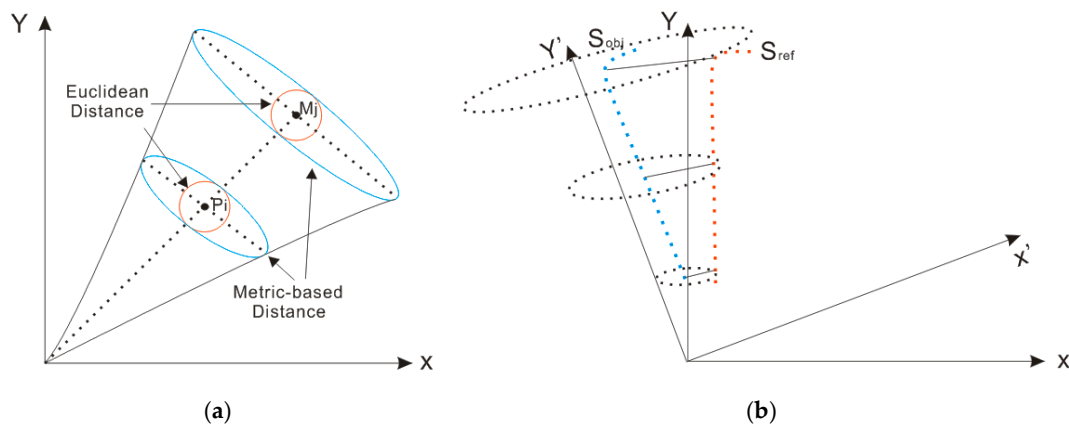


Figure 3. (a) Iso-distance curves: the blue curve is from the metric-based distance, and the red curve is from the Euclidean distance; (b) associations between scans with large scans that are built by the metric-based distance.

2.3. Resampling

Laser scanners have a settled viewing angle and resolution, so a longer scanning distance increases the distance between neighboring scanned points. When a mobile robot moves forward in a long narrow corridor, the density distribution of point clouds from the laser scanner greatly varies according to the distance from the sensor. Sensors scan fewer points at greater distances (as shown in Figure 4a). However, such a different density distribution of point clouds may slow down the iteration process and distort the calculation of the rejection threshold, as mentioned in chapter 2.4.1. Therefore, we utilize a resampling method that is based on grid partitioning to realize a relatively even density distribution.

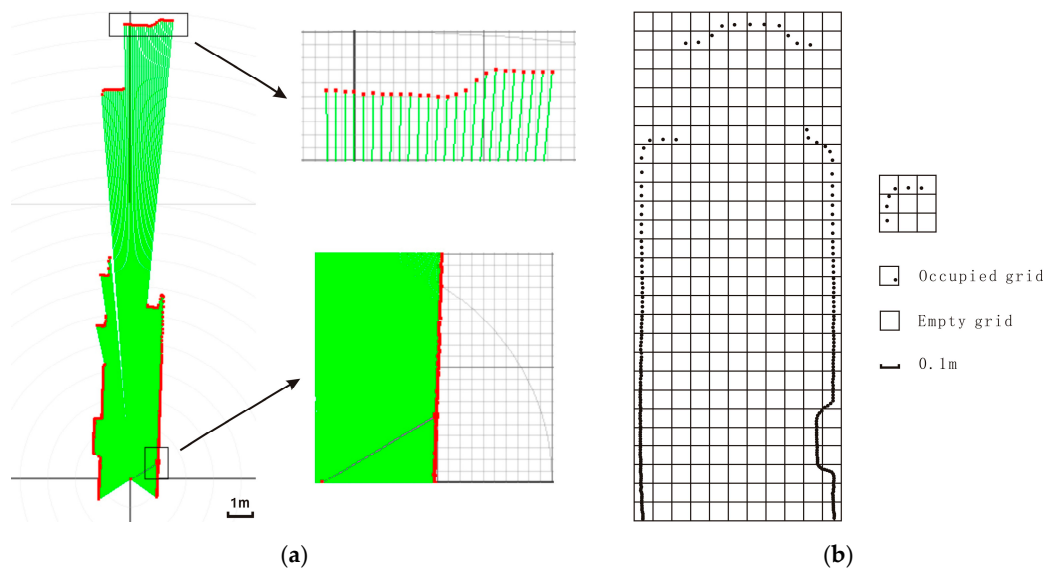


Figure 4. (a) Different density distributions of point clouds; (b) spatial partition.

First, we build a spatial grid for the object point cloud. We use a coordinate system that is centered at the sensor’s position to calculate the coordinates of all the scanned points and then obtain the minimum bounding rectangle of the point cloud. The rectangle is partitioned into grids according to a given grid length (0.1 m is used according to the sensor’s resolution), as shown in Figure 4b.

Second, we calculate a sampling percentage for points in each grid. Given two occupied grids whose row and column indices are (r_1, c_1) and (r_2, c_2) , respectively, the distance d between the grids is

defined as $\sqrt{(r_1 - r_2)^2 + (c_1 - c_2)^2}$. The sensor is contained in the center grid, so its row and column indices are both zero. We calculate the distance d_i from each grid to the center grid according to the distance definition and obtain the max distance (d_{max}). The sampling ratio for points in each grid is thus defined as the ratio of d_i and d_{max} , which guarantees that distant grids from the center grid have a relatively high sampling percentage and nearby grids have a low sampling percentage.

Finally, we resample points in the units of the grids according to the assigned sampling percentage. Given a grid with n points and sampling percentage η , the sampling size n' is calculated as the ceiling of $n \times \eta$. To preserve as much topological information as possible for the points, the first and last points are preserved and the remaining $n' - 2$ points are sampled at regular intervals, as shown in Figure 5a.

This resampling method is based on a grid partition, which determines the sampling percentage according to the distance from the occupied grid to the center grid and then samples points in the units of the grid according to the topological information. This method can effectively dilute dense points nearby and retain their topological information, therefore accelerating the iteration process and preventing the calculation of the rejection threshold from becoming distorted by the greatly varying density distributions of point clouds.

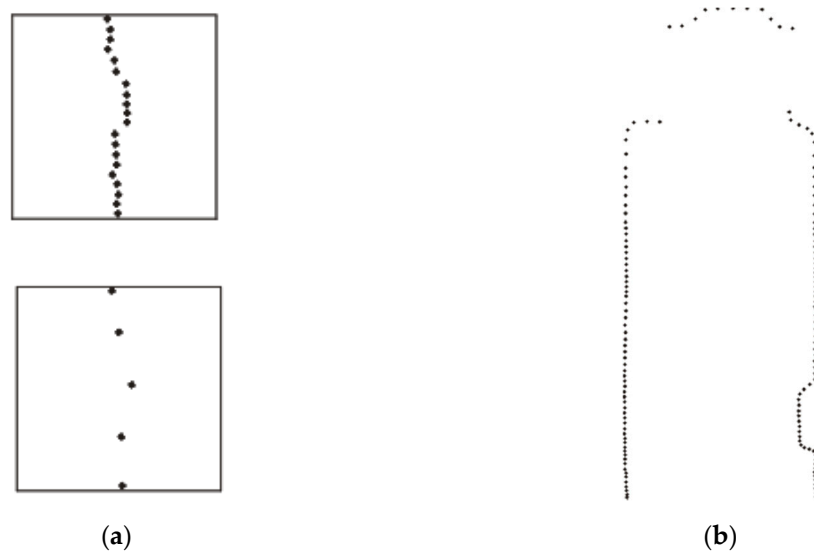


Figure 5. (a) Resampling process in grid form; (b) resampled point clouds.

2.4. Improved MbICP Algorithm

2.4.1. Correspondence Establishment

The MbICP algorithm finds correspondence points by finding the nearest point through its defined metric-based distance, which is claimed to perform better than when using the Euclidean distance when large rotation exists. However, this algorithm is still based on a point-to-point metric, which is not as reliable because of mismatching from partial overlapping and the discreteness of laser scans. For example, given two successive laser scans that are captured at the beginning and end of robot motion, partial overlapping can be clearly observed in rectangular area 1 in Figure 6a,b. This area contains no actual correspondence points for points in the object scan, thus producing many incorrect correspondences. Additionally, different points in the object scan incorrectly correspond to the same point in the reference scan because of the discrete nature of the scan, as shown in rectangular area 2 in Figure 6a. These incorrect correspondences will distort the follow-up calculation of the optimal transformation and thus negatively affect the final matching result.

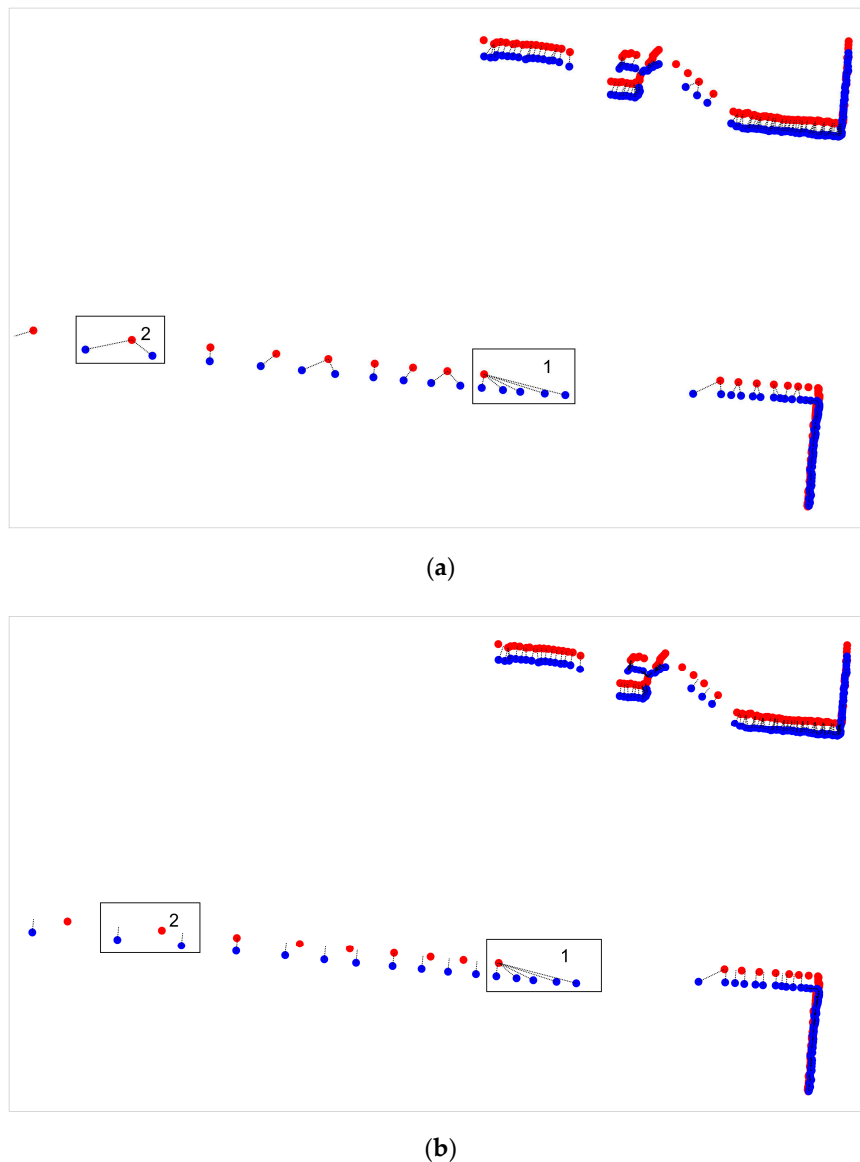


Figure 6. (a) Correspondences that were established based on the point-to-point metric (red dots-reference scan, blue dots-object scan, black lines-correspondences); (b) correspondences that were established based on the point-to-line metric (red dots-reference scan, blue dots-object scan, black lines-correspondences).

To reduce problems that are introduced by the point-to-point metric, this paper improves the procedure of determining the correspondence by combining the point-to-point and point-to-line metrics. First, the nearest point m_j in the reference scan is determined for each point p_i in the object scan by using the metric-based distance, and (p_i, m_j) is treated as a candidate correspondence pair. For those candidate correspondence pairs whose object points correspond to a reference point, only the pair with the smallest corresponding distance is preserved and the remaining pairs are modified by using an interpolation method. Taking (p_i, m_j) as an example, we search for the second-closest point m'_j for p_i in the reference scan, and a segment that begins at m_j and ends at m'_j is found. We calculate the projection of p_i onto the segment along the normal and use this interpolation point as a new corresponding point (as shown in Figure 7a). This interpolation is less risky because it only utilizes the surface information of the reference point clouds.

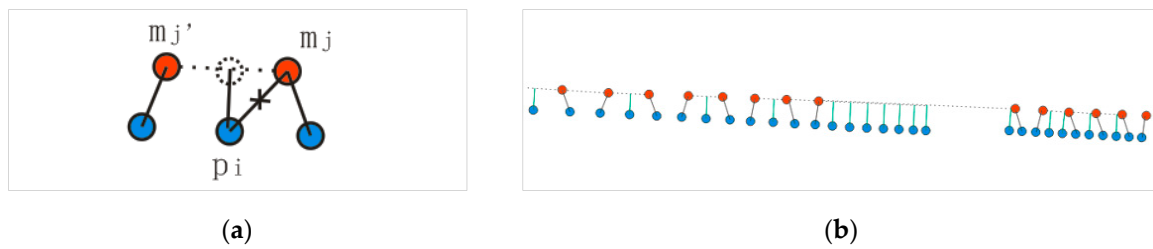


Figure 7. (a) Interpolation process (red dots-scanned points in reference scan, blue dots-scanned points in object scan); (b) correspondences that were established by the new procedure (red dots-scanned points in reference scan, blue dots-scanned points in object scan).

This new procedure can improve the performance of correspondence establishment, especially when non-overlapping areas exist (as shown in Figure 8). However, a few incorrect correspondence pairs might be established because of the complexity of the environment. Thus, a rejection strategy will be explained in the next section.

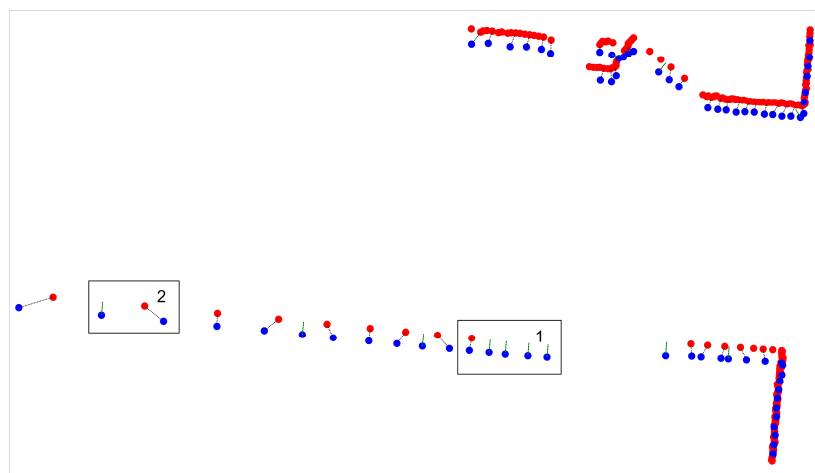


Figure 8. Correspondences that were established based on the new procedure (red dots-reference scan, blue dots-object scan).

2.4.2. Rejection of Incorrect Correspondences

After establishing correspondence based on the new procedure, a set of correspondence pairs are obtained, which may contain a few incorrect correspondence pairs with large distance. Therefore, a rejection strategy that is based on the corresponding distance is required to protect the follow-up calculation from transformation.

One of the most commonly used methods is the standard-deviations-from-mean approach, which removes values that are more than n standard deviations from the mean. The value of n is decided according to the practical situation. However, this method is unreliable because extreme values may distort the mean and standard deviation.

For example, given a sequence of correspondence distances, $X = \{12.281, 12.270, 12.712, 11.932, 11.053, 10.768, 11.077, 11.685, 6.393, 6.001, 5.549, 38.760, 86.305, 34.497, 2.988, 3.227, 1.297, 3.539, 6.409, 12.477, 12.381\}$. The rejection result when using the standard-deviations-from-mean approach is depicted in a dot plot (as shown in Figure 9a). The mean is approximately 14.93, which obviously deviates from the center of the data set, and the standard deviation is also considerably distorted. Only 86.305 is rejected as an extreme value, while 38.760 and 34.497 are ignored even though they are obviously also extreme values.

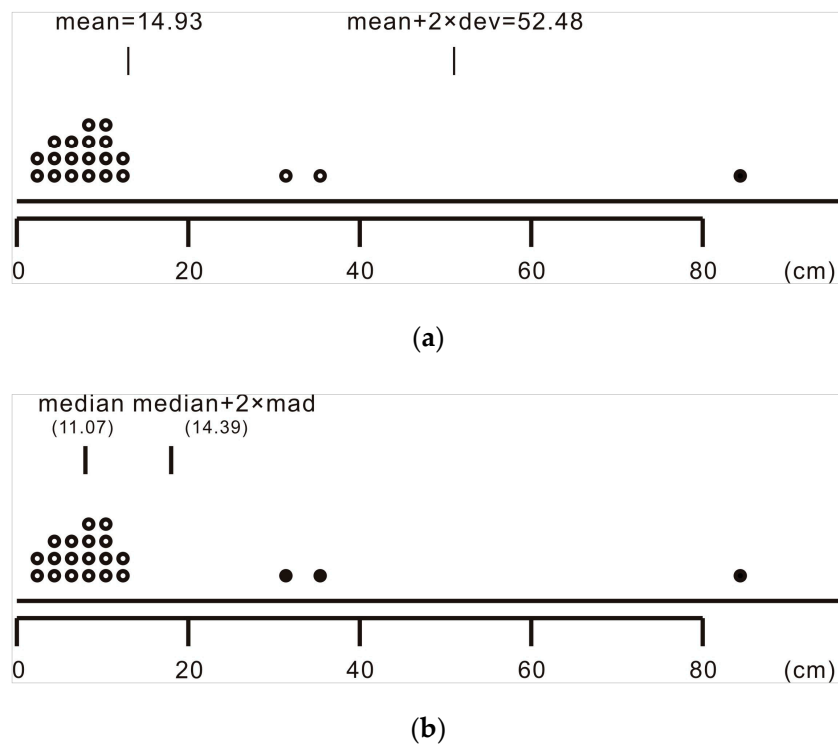


Figure 9. (a) Rejection result via the standard-deviations-from-mean approach; (b) rejection result via the MAD-from-median method.

The MAD-from-median method is another rejection method, which removes values that are more than two median absolute deviations (MAD) from the median. Instead of utilizing the mean and standard deviation to measure the center and discreteness degree of the data set, this method uses the median and MAD to represent the clustering and statistical dispersion of the data set. The median is not greatly skewed by extreme values and thus can provide a better idea of the typical value than the mean can. The MAD, which is defined as the median of the absolute deviations from the median of the data set, is also robust to extreme values.

The rejection result when using the MAD-from-median method is depicted in Figure 9b. The median is 11.07, which is a good representation of the center. Here, 38.760, 86.305 and 34.497 are all rejected as extreme values. Thus, the MAD-from-median method can more clearly differentiate extreme values and is herein adopted to reject correspondences with large distances.

$$d_{rej} = \text{median}(X) + 2 \times MAD \tag{5}$$

Therefore, we calculate the rejection threshold d_{rej} by using Equation (5) and reject correspondences with distances above d_{rej} , which are likely incorrect correspondences. This rejection strategy is risky because d_{rej} may be distorted by the greatly varying density distributions of point clouds. When a mobile platform moves forward in a long narrow corridor, point clouds tend to be quite dense near the sensor but sparse in more distant regions from the sensor. However, the object point clouds cannot be moved closer to the reference point clouds because of the absence of an initial pose from the odometer. The dense points that are distributed within the corridor (rectangle 2 in Figure 10a) can hardly find actual correspondence points and are likely to establish incorrect correspondences with minor distances, which are unhelpful but are in the majority. The sparse points that are distributed within the frontal obstacles (rectangle 1 in Figure 10a) are likely to establish correct correspondences with relatively large distances, which are vital to bring two point clouds closer but are in the minority. Therefore, directly rejecting correspondence pairs that have distances above d_{rej} but that are vital for

calculating the transformation, may cause potential local-minima problems. Fortunately, this risk is reduced by the resampling method in chapter 2.3, so d_{rej} can effectively reject correspondences with extremely large distances and preserve vital correct correspondences (rectangle 1 in Figure 10b).

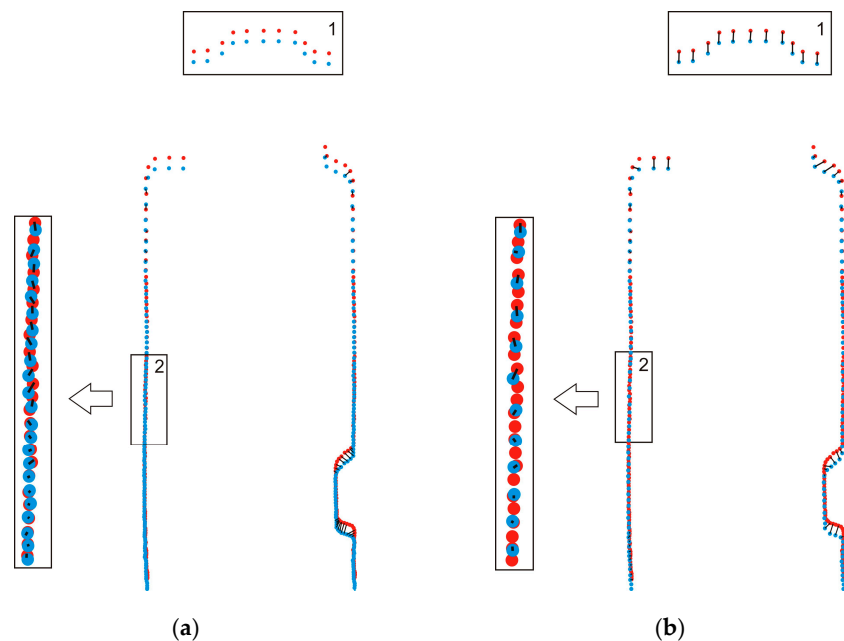


Figure 10. (a) Rejection result without the resampling step (red dots-reference scan, blue dots-object scan, black lines-correspondences); (b) rejection result with the resampling step (red dots-reference scan, blue dots-object scan, black lines-correspondences).

3. Results

The experimental results are outlined in this section. We tested the improved MbICP algorithm with data from a mobile wheelchair platform that was equipped with a Hokuyo UTM-30LX laser range finder (Hokuyo Co. Ltd., Osaka, Japan). The Hokuyo UTM-30LX is a 2-D laser range finder with a 30 m effective measurement range, 270° field of view (angular resolution of 0.25°), and 40 Hz scanning rate. We designed two types of experiments to compare our algorithm with the original algorithm. The first experiment evaluated the properties of the algorithms by matching a pair of scans that partially overlapped. The second experiment evaluated the global algorithm performance with a run within our academic building.

3.1. Evaluation Method

The first experiment compared the accuracy and convergence of the improved MbICP algorithm with those of the original MbICP algorithm in matching partially overlapped scans. Before introducing more details regarding the experiment, we first explain the evaluation factors of the accuracy and convergence. Given two scans that were acquired in the same sensor location, we precisely know that the ground truth of the pose estimate is $(0, 0, 0^\circ)$. To quantitatively compare the algorithms' accuracy, a random displacement δ is added to the initial pose estimate, and one scan is also roto-translated by this value. This transformed scan is treated as the object scan, which is marked as S_{obj} , while the other scan is treated as the reference scan, which is marked as S_{ref} . After matching, the pose estimation is determined and statistical analysis can be performed. The translational and rotational deviation between the pose estimation from the algorithm and the ground truth is used as the evaluative factor of the algorithm's accuracy. The smaller the deviation, the more closely S_{obj} fits S_{ref} and the better the accuracy of the algorithm. In addition, the number of iterations can intuitively represent the algorithm's convergence.

We conducted the first experiment by matching two partially overlapping scans with the improved algorithm and standard algorithm. To obtain experimental scans, we recorded data taken by UTM-30LX laser range finder in a corner by artificially adding or removing the trashcan in the field of view without moving the sensor. This way we acquired a pair of scans that partially overlap, one of which with the presence of the trashcan is shown in Figure 11a and the other is shown in Figure 11b. The scan with this trashcan was roto-translated with a given transformation (500 mm, 500 mm, 15°) and then used as the object scan, while the scan without the trashcan was treated as the reference scan (as shown in Figure 12a). The matching result from the standard algorithm is depicted in Figure 12b, which is far from satisfactory because of obvious deviation between two scans. The distance between the estimated pose and the ground truth was (75.75 mm, 34.69 mm, 2.71°), demonstrating awful accuracy. However, the matching result from the improved algorithm was relatively satisfactory because the two scans closely matched (as shown in Figure 12c). The deviation between the estimated pose and ground truth was nearly zero, demonstrating high accuracy. The improved algorithm also exhibited a faster convergence rate (18 iterations) because of the resampling step, while the standard algorithm satisfied the convergence condition after 22 iterations (Figure 12d).

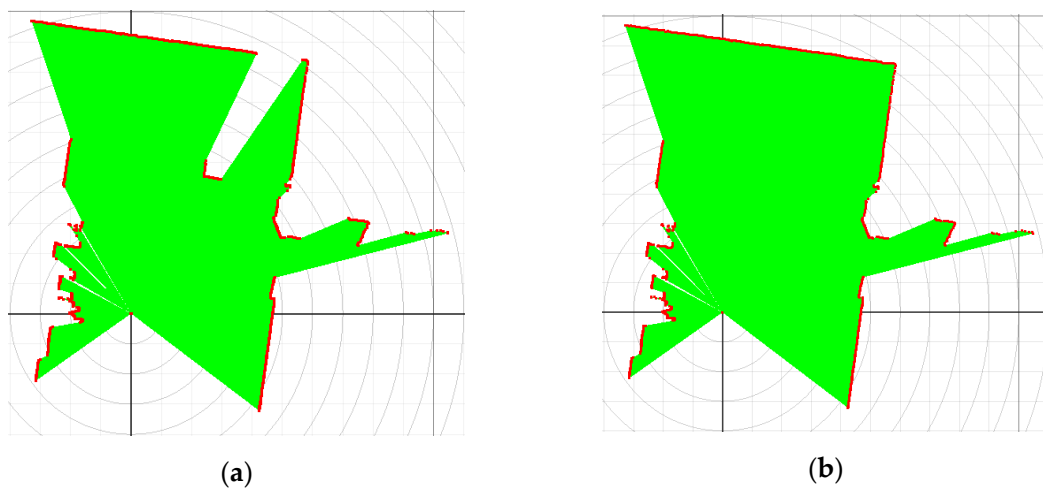


Figure 11. Two partially overlapping scans taken by sensor at the same location: (a) The first scan was captured with the presence of a trashcan; (b) the second scan was captured without the presence of a trashcan.

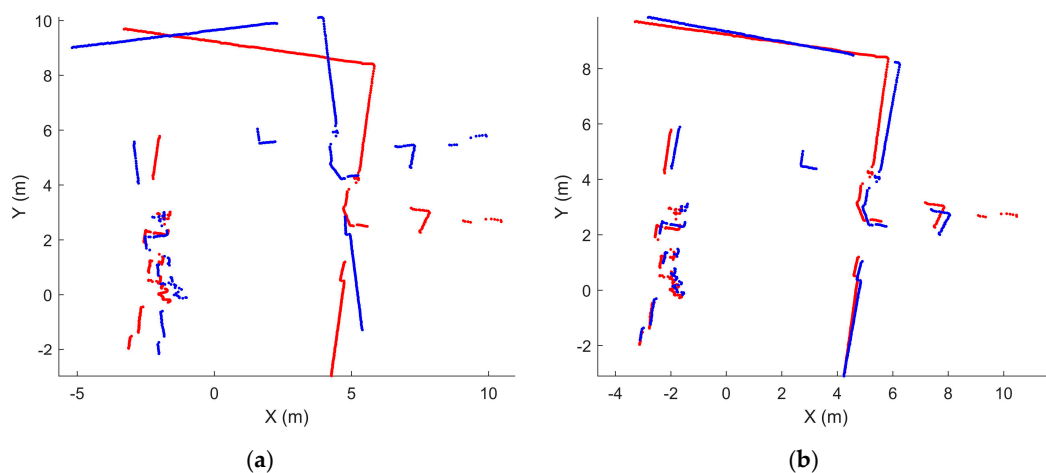


Figure 12. Cont.

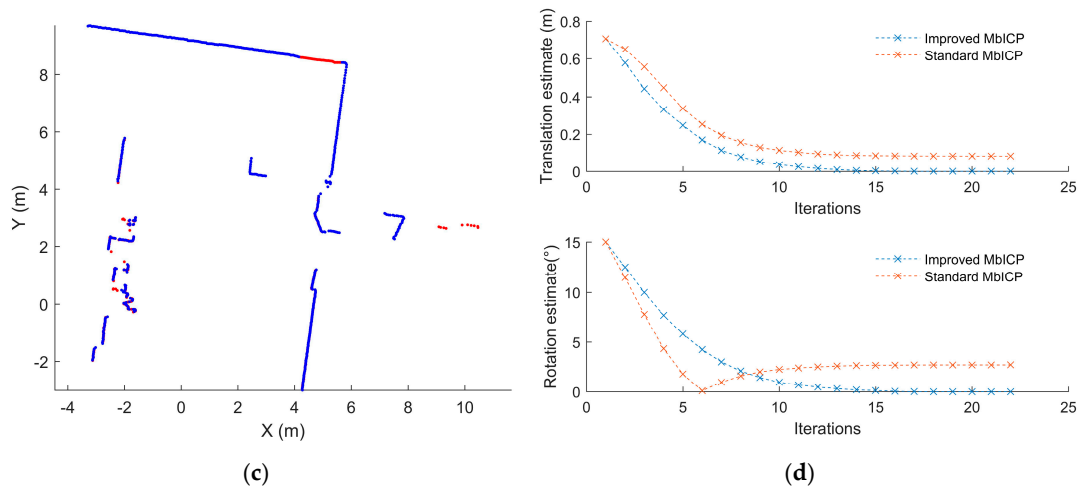


Figure 12. (a) Object scan (blue) and reference scan (red); (b) matching result from the standard MbICP algorithm (red dots-reference scan, blue dots-transformed object scan); (c) matching result from the improved MbICP algorithm (red dots-reference scan, blue dots-transformed object scan); (d) iteration process.

Another group of experiments was conducted to quantitatively evaluate the algorithms' accuracy in matching scans with different overlapping ratios. Given an overlapping percentage $\eta\%$ and two identical scans, one scan had $1 - \eta\%$ of the points artificially removed, while the other scan remained unchanged from the object scan. Thus, we obtained pairs of scans with an overlapping percentage η , which varied from 60% to 100%. These scans were acquired under different scenarios, such as stairs and corners, where overlapping frequently occurs because of range holes and rotation, and corridors, where dynamic obstacles are common (as shown in Figure 13). We repeated each matching experiment 10 times with these two algorithms for each overlapping percentage and each scenario (a total of 400 runs), and the common parameters were identical.

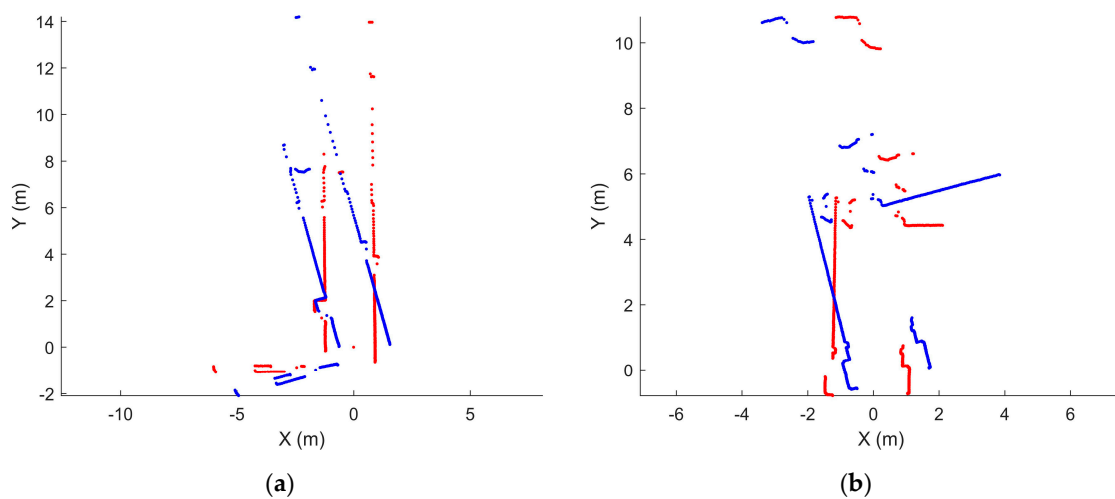


Figure 13. Cont.

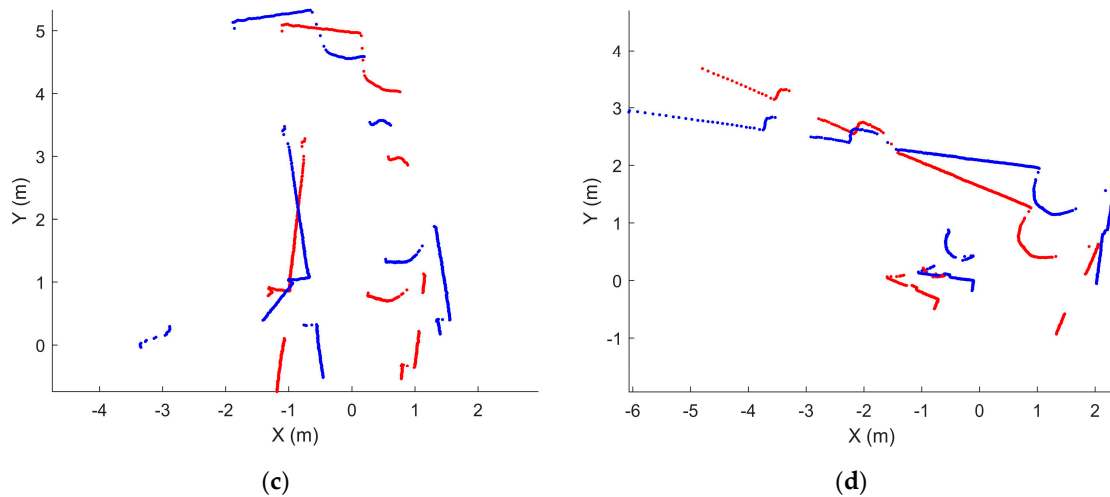


Figure 13. (a) Scans obtained in corridor 1 (red dots-reference scan, blue dots-object scan); (b) scans obtained near stairs (red dots-reference scan, blue dots-object scan); (c) scans obtained in corridor 2 (red dots-reference scan, blue dots-object scan); (d) scans obtained in the corner (red dots-reference scan, blue dots-object scan).

We first discuss the results in terms of robustness. A scan match was considered a failure when the solution was larger than 0.1 m in translation and 3.14° in rotation. Solutions with an error below the threshold were used in a follow-up precision analysis. *True Positives* (converged to the right solution), *False Positives* (converged to an incorrect solution), *True Negatives* (not converged but the solution is correct) and *False Negatives* (not converged and the solution is incorrect) are frequently used robustness characteristics.

For the standard algorithm, the true positives decreased and the false positives increased as the overlapping percentage decreased, as shown in Table 1. Thus, the robustness of the standard algorithm was influenced by non-overlapping areas between scans. The improved algorithm showed good robustness because all the solutions were true positives despite a decrease in the overlapping percentage, as shown in Table 2.

Table 1. Solutions that were generated by the standard algorithm.

Overlapping Ratio (%)	Solutions (%)			
	True Positive	False Positive	True Negative	False Negative
100	100	0	0	0
90	100	0	0	0
80	90	10	0	0
70	70	25	0	5
60	55	37.5	0	7.5

Table 2. Solutions that were generated by the improved algorithm.

Overlapping Ratio (%)	Solutions (%)			
	True Positive	False Positive	True Negative	False Negative
100	100	0	0	0
90	100	0	0	0
80	100	0	0	0
70	92.5	7.5	0	0
60	90	7.5	0	2.5

We calculated the deviation between the estimated pose and ground truth to indicate the precision (only using *True Positives*), as shown in Table 3. Both algorithms were accurate when two scans perfectly overlapped but experienced increasing deviation in their translation and rotation as the overlap ratio decreased. However, the improved algorithm was more accurate than the standard algorithm when the scans partially overlapped. Moreover, a decline in the overlap ratio substantially decreased the performance of the standard algorithm but had no significant effect on the improved algorithm.

Table 3. Deviation in the translation and rotation.

Overlapping Ratio (%)	Translation Error (mm)		Rotation Error (°)	
	Improved	Standard	Improved	Standard
100	0	0	0	0
90	1.373	6.518	0.022	0.279
80	5.289	38.940	0.113	0.832
70	12.142	43.226	0.283	1.528
60	18.582	64.040	0.657	1.892

3.2. Real-World Applications

The first experiment was ingenious because it allows for matching real-world scans without requiring the ground truth, but generating scans with a specific overlapping percentage by randomly removing a certain number of points is risky and does not always conform to reality. Therefore, we conducted a second experiment, which involved a run with a mobile robot on the 4th floor of the School of Resource and Environment Science Building, Wuhan University. This building consisted of three narrow corridors and two corners, forming a U-shaped room. Stationary structures, such as offices, stairs and toilets, were distributed along the corridors. In addition, dynamic obstacles such as umbrellas and walking people were present in this scenario. We applied the two algorithms to match each pair of successive scans and output many transformed cloud points and a trajectory. This experiment was challenging because the overlapping percentage of successive scans from rotation and range holes could not be estimated in advance.

Figure 14 depicts the matching results from the two algorithms. Obtaining the exact transformation data for each step during the experiment was difficult [1]. The ground truth and numeric values are thus actually unavailable in real-world applications because of a lack of information regarding actual robot poses, which is commonly the case in current relevant studies [1,10]. The results of the improved algorithm were clearly better than those of the standard algorithm because the former could adequately fit successive scans and the generated point clouds accurately presented the indoor structure. In contrast, the matching results from the standard algorithm suffered from several obvious mismatches around stairs and corners. Thus, the behavior of the improved algorithm was generally better than that of the standard algorithm under more realistic conditions.

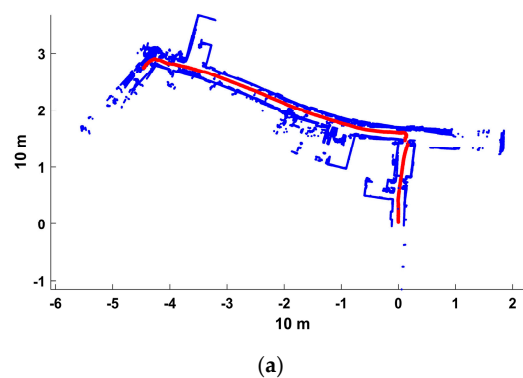


Figure 14. Cont.

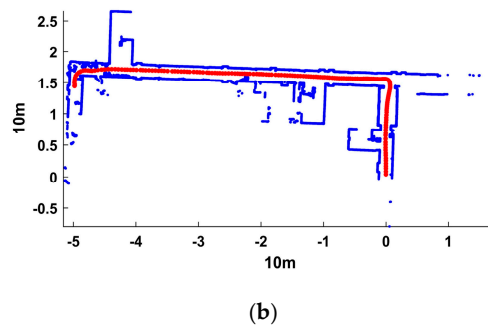


Figure 14. (a) Matching result from the standard MbICP algorithm; (b) matching result from the improved MbICP algorithm.

3.3. Discussion

The improved MbICP algorithm is limited in that it may fall into local minima under specific scenarios, such as a long, narrow corridor with few frontal structures, indicating the need for further improvement. Frontal obstacles are very vital to bring two clouds together because their correspondences play an important role in calculating a ground transformation. As seen in Figure 15a, the left scan was captured in a long narrow corridor (corresponding to rectangle 2 in Figure 15b) where there are few frontal obstacles, while the right scan was captured in a long narrow corridor (corresponding to rectangle 1 in Figure 15b) where there are several frontal obstacles. As seen in Figure 15b, the matching result was satisfactory in rectangle 1 but demonstrated a “shortening” effect in rectangle 2. Bringing two point clouds closer was difficult because of lacking necessary frontal obstacles and insufficient correct correspondences that are vital for gaining an optimal transformation in each iteration, thus causing local-minima problems.

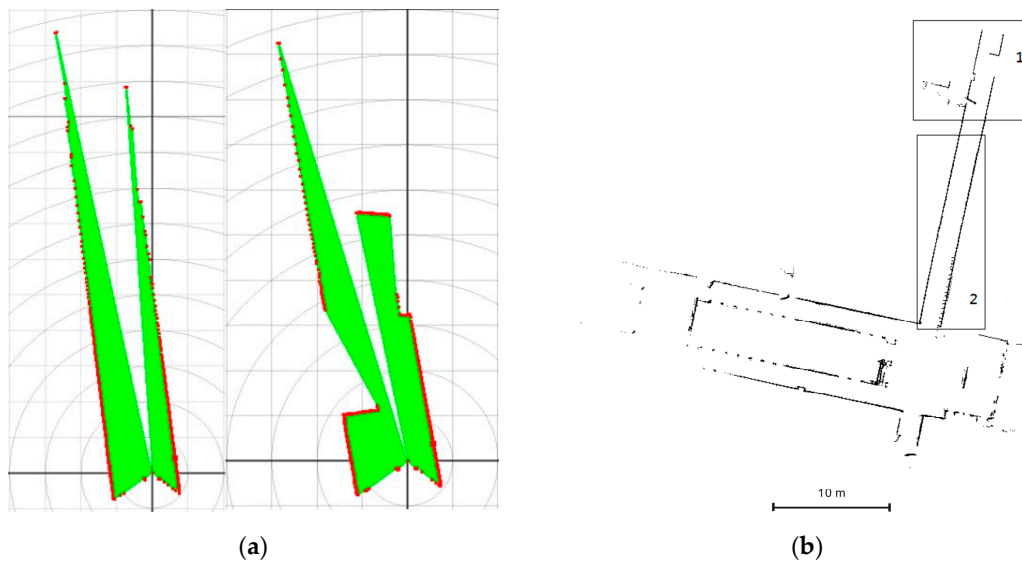


Figure 15. (a) The left scenario is a corridor without frontal obstacles, and the right scenario is a corridor with frontal obstacles; (b) matching result for scans from a long narrow corridor, with frontal obstacles in rectangle 1 and few frontal obstacles in rectangle 2.

4. Conclusions

This paper presented an improved MbICP algorithm to estimate robot motion to overcome this method’s inability to match partially overlapping 2D scans. A resampling step was executed to smooth the greatly varying density distributions of point clouds, which could accelerate the iteration

process and protect the follow-up rejection method from becoming distorted. Then, correspondences were established by an improved procedure that combined the simplicity of the point-to-point metric and accuracy of the point-to-line metric. Finally, a rejection threshold that was based on a MAD-from-median approach was used to discard correspondences with large distances, which were likely incorrect correspondences. The results of the first experiment demonstrated that both algorithms were disturbed by a decrease in the overlapping percentage, but the improved algorithm still exhibited better accuracy and robustness. The results of the second experiment indicated that the improved algorithm is valid in practice and exhibits better performance than the standard algorithm.

In future work, our method needs further improvement to be applied under more scenarios, including long and narrow corridors where frontal obstacles are rare. Utilizing geometric features of the point cloud, such as curvature, normal and density, is a possible solution. In addition, how our method could be extended to the scan matching of 3D point clouds needs further consideration.

Acknowledgments: This study is funded by the National Key R&D Program of China (2017YFB0503701), the Scientific and Technological Leading Talent Fund of the National Administration of Surveying, Mapping and Geo-information (2014) and the Wuhan ‘Yellow Crane Excellence’ (Science and Technology) program (2014).

Author Contributions: This study was completed by the co-authors, and the major experiments and analyses were undertaken by Jun Liu. Lin Li supervised and guided this study, Haihong Zhu designed the proposal for the experiments and conducted the analyses, Xinkai Zuo aided in the collection and analysis of the data, and Jun Liu wrote the paper. All the authors have read and approved the final manuscript.

Conflicts of Interest: The authors declare no conflicts of interest.

References

1. Lv, J.; Yukinori, K.; Ravankar, A.A.; Ravankar, A.; Emaru, T. A solution to estimate robot motion with large rotation by matching laser scans. In Proceedings of the 54th Annual Conference of the Society of Instrument and Control Engineers of Japan, Hangzhou, China, 28–30 July 2015.
2. Liu, Y.; Sun, Y. Mobile robot instant indoor map building and localization using 2d laser scanning data. In Proceedings of the International Conference on System Science and Engineering, Dalian, China, 30 June–2 July 2012.
3. Yin, J.; Carlone, L.; Rosa, S.; Anjum, M.L.; Bona, B. Scan matching for graph slam in indoor dynamic scenarios. In Proceedings of the International Conference of the Florida Artificial Intelligence Research Society, Pensacola Beach, FL, USA, 21–23 May 2014.
4. Diosi, A.; Kleeman, L. Fast laser scan matching using polar coordinates. *Int. J. Rob. Res.* **2007**, *26*, 1125–1153. [[CrossRef](#)]
5. Dissanayake, M.W.M.G.; Newman, P.; Clark, S.; Durrant-Whyte, H.F.; Csorba, M. A solution to the simultaneous localization and map building (slam) problem. *IEEE Trans. Rob. Autom.* **2001**, *17*, 229–241. [[CrossRef](#)]
6. Berns, K.; Puttkamer, E.V. *Simultaneous Localization and Mapping (Slam)*; Springer: Berlin, Germany, 2009; pp. 146–172.
7. Pedrosa, E.; Pereira, A.; Lau, N. Efficient localization based on scan matching with a continuous likelihood field. In Proceedings of the IEEE International Conference on Autonomous Robot Systems and Competitions, Coimbra, Portugal, 26–28 April 2017.
8. Wang, X.; Jia, Y.; Xi, N.; Zhen, J.; Xu, F. Mobile robot pose estimation using laser scan matching based on fourier transform. In Proceedings of the IEEE International Conference on Robotics and Biomimetics, Bali, Indonesia, 5–10 December 2014.
9. Park, S.; Park, S.K. Global localization for mobile robots using reference scan matching. *Int. J. Control Autom. Syst.* **2014**, *12*, 156–168. [[CrossRef](#)]
10. Minguez, J.; Montesano, L.; Lamiroux, F. Metric-based iterative closest point scan matching for sensor displacement estimation. *IEEE Trans. Rob.* **2006**, *22*, 1047–1054. [[CrossRef](#)]
11. Montesano, L.; Minguez, J.; Montano, L. Probabilistic scan matching for motion estimation in unstructured environments. In Proceedings of the IEEE/RSJ International Conference on Intelligent Robots and Systems, Edmonton, AB, Canada, 2–6 August 2005.

12. Burguera, A.; Oliver, G.; Tardos, J.D. Robust scan matching localization using ultrasonic range finders. In Proceedings of the IEEE/RSJ International Conference on Intelligent Robots and Systems, Edmonton, AB, Canada, 2–6 August 2005.
13. Park, S.; Kim, D.H.; Park, M.; Park, S.K. Spectral scan matching for robot pose estimation. *Electron. Lett.* **2009**, *45*, 1076–1077. [[CrossRef](#)]
14. Pfister, S.T.; Kriechbaum, K.L.; Roumeliotis, S.I.; Burdick, J.W. Weighted range sensor matching algorithms for mobile robot displacement estimation. In Proceedings of the IEEE International Conference on Robotics and Automation, Washington, DC, USA, 11–15 May 2002.
15. Bengtsson, O.; Baerveldt, A.J. Localization by matching of range scans—Certain or uncertain? In Proceedings of the Eurobot'01—Fourth European Workshop on Advanced Mobile Robots, Lund, Sweden, 19–21 September 2001.
16. Feng, L.; Milios, E. Robot pose estimation in unknown environments by matching 2d range scans. *J. Intell. Robot. Syst.* **1997**, *18*, 249–275.
17. Jensen, B.; Siegwart, R. Scan alignment with probabilistic distance metric. In Proceedings of the IEEE/RSJ International Conference on Intelligent Robots and Systems, Sendai, Japan, 28 September–2 October 2004.
18. Donoso, F.A.; Austin, K.J.; McAree, P.R. How do ICP variants perform when used for scan matching terrain point clouds? *Robots Autom. Syst.* **2017**, *87*, 147–161. [[CrossRef](#)]
19. Pomerleau, F.; Colas, F.; Siegwart, R.; Magnenat, S. Comparing ICP variants on real-world data sets. *Auton. Robots* **2013**, *34*, 133–148. [[CrossRef](#)]
20. Zhang, L.; Choi, S.I.; Park, S.Y. Robust icp registration using biunique correspondence. In Proceedings of the International Conference on 3d Imaging, Modeling, Processing, Visualization and Transmission, Hangzhou, China, 16–19 May 2011.
21. Zhu, J.; Zheng, N.; Yuan, Z.; Du, S. Point-to-line metric based iterative closest point with bounded scale. In Proceedings of the 4th IEEE Conference on Industrial Electronics and Applications, Xian, China, 25–27 May 2009.
22. Pomerleau, F.; Colas, F.; Ferland, F.; Michaud, F. *Relative Motion Threshold for Rejection in ICP Registration*; Springer: Berlin/Heidelberg, Germany, 2009; pp. 229–238.
23. Phillips, J.M.; Liu, R.; Tomasi, C. Outlier robust icp for minimizing fractional rmsd. In Proceedings of the Sixth International Conference on 3-D Digital Imaging and Modeling, Montreal, QC, Canada, 21–23 August 2007.
24. Zhu, J.; Meng, D.; Li, Z.; Du, S.; Yuan, Z. Robust registration of partially overlapping point sets via genetic algorithm with growth operator. *IET Image Proc.* **2014**, *8*, 582–590. [[CrossRef](#)]
25. Kim, H.Y.; Lee, S.O.; You, B.J. Robust laser scan matching in dynamic environments. In Proceedings of the 2009 IEEE International Conference on Robotics and Biomimetics, Guilin, China, 19–23 December 2009.
26. Chetverikov, D.; Svirko, D.; Stepanov, D.; Krsek, P. The trimmed iterative closest point algorithm. In Proceedings of the 16th International Conference on Pattern Recognition, Quebec City, QC, Canada, 11–15 August 2002.
27. Chen, Y.; Medioni, G. Object modeling by registration of multiple range images. In Proceedings of the IEEE International Conference on Robotics and Automation, Sacramento, CA, USA, 9–11 April 1991.
28. Rusinkiewicz, S.; Levoy, M. Efficient variants of the ICP algorithm. In Proceedings of the Third International Conference on 3-D Digital Imaging and Modeling, Quebec City, QC, Canada, 28 May–1 June 2001.
29. Druon, S.; Aldon, M.J.; Crosnier, A. Color constrained ICP for registration of large unstructured 3d color data sets. In Proceedings of the IEEE International Conference on Information Acquisition, Seogwipo-si, Korea, 8–11 July 2007.
30. Zinsser, T.; Schmidt, J.; Niemann, H. A refined ICP algorithm for robust 3-d correspondence estimation. In Proceedings of the International Conference on Image Processing, Barcelona, Spain, 14–17 September 2003.
31. Arun, K.S.; Huang, T.S.; Blostein, S.D. Least-squares fitting of two 3-d point sets. *IEEE Trans. Pattern Anal. Mach. Intell.* **2009**, *PAMI-9*, 698–700. [[CrossRef](#)]

